PCCP

ROYAL SOCIETY OF CHEMISTRY

PAPER

View Article Online
View Journal | View Issue

Cite this: *Phys. Chem. Chem. Phys.*, 2024, **26**, 5156

A molecular descriptor of a shallow potential energy surface for the ground state to achieve narrowband thermally activated delayed fluorescence emission†

Jiaqiang Zhao,[a] Huanling Liu,[b] Jianzhong Fan *[b] and Qingfang Mu*[b]

Narrowband thermally activated delayed fluorescence (TADF) molecules have extensive applications in optoelectronics, biomedicine, and energy. The full-width at half-maximum (FWHM) holds significant importance in assessing the luminescence efficiency and color purity of TADF molecules. The goal is to achieve efficient and stable TADF emissions by regulating and optimizing the FWHM. However, a bridge from the basic physical parameters (such as geometric structure and reorganization energy) to the macroscopic properties (delayed fluorescence, efficiency, and color purity) is needed and it is highly necessary and urgent to explore the internal mechanisms that influence FWHM. Herein, first-principles calculations coupled with the thermal vibration correlation function (TVCF) theory were performed to study the energy consumption processes of the excited states for the three TADF molecules (2,3-POA, 2,3-DPA, and 2,3-CZ) with different donors; inner physical parameters affecting the FWHM were detected. By analyzing the basic geometric and electronic structures as well as the transition properties and reorganization energies, three main findings in modulating FWHM were obtained, namely a large local excitation (LE) proportion in the first singlet excited state is advantageous in reducing FWHM, a donor group with weak electron-donating ability is beneficial for achieving narrowband emission, and small reorganization energies for the ground state are favorable for reducing FWHM. Thus, wise molecular design strategies to achieve efficient narrowband TADF emission are theoretically proven and proposed. We hope that these results will promote an in-depth understanding of FWHM and accelerate the development of high color purity TADF emitters.

Received 2nd December 2023,
Accepted 4th January 2024

DOI: 10.1039/d3cp05875a

rsc.li/pccp

1. Introduction

In recent years, with the thriving development of thermally activated delayed fluorescence (TADF) materials, the research interest in TADF molecules has rapidly escalated.[1–5] TADF molecules have become a research hotspot in organic light-emitting diodes (OLEDs) due to their advantages of 100% internal quantum efficiency and the absence of precious metals.[6–10] Although the efficiency of TADF molecules has greatly improved, high color purity remains a key issue that needs to be addressed.[11–17] Organic luminescence molecules typically exhibit strong vibrational relaxation (with rates ranging from 10^{12} to 10^{15} s^{-1}) and strong vibrational coupling between the excited state and ground state; as a result, their emission spectra are relatively broad, and developing narrowband TADF molecules is a longstanding challenge in the field of electroluminescence.[18–24]

Researchers have made great efforts in this field. For the first time, Duan *et al.* reported a series of efficient green-emitting multi-resonance induced thermally activated delayed fluorescence (MR-TADF) materials by amplifying the influence of the skeleton and peripheral units. Peripheral units with electron-deficient characteristics could significantly reduce the highest occupied molecular orbital (HOMO) and the lowest unoccupied molecular orbital (LUMO) energy gap while maintaining color purity. Thus, an MR-TADF emitter with a photoluminescence quantum yield of over 90% and a full-width at half-maximum (FWHM) of 25 nm was developed.[25] Woo *et al.* synthesized a series of green fluorescence moieties based on a tetra-azaacene core by introducing nitrile substituents at different positions. Corresponding results showed that the

[a] *School of Physics and Electronic Information, Weifang University, Weifang 261061, China. E-mail: qingfangmusdnu@163.com*
[b] *Shandong Province Key Laboratory of Medical Physics and Image Processing Technology, Institute of Materials and Clean Energy, School of Physics and Electronics, Shandong Normal University, Jinan 250014, China. E-mail: fanjianzhongvip@163.com*

† Electronic supplementary information (ESI) available. See DOI: https://doi.org/10.1039/d3cp05875a

molecular structure of organic fluorescence moieties could be modulated by adjusting the structure and position of the substituents, thereby suppressing the narrowband emission from the ν_{0-n} (n = 1, 2, 3...) vibrational transition.[26] Zhang and Adachi proposed an ultrapure green emitter of 11,16,28,33,39-pentakis(2-methylprop-2-yl)-19,36-dibora-1,7,24-triazatridecacyclo[21.19.2.12,6.17,18.124,35.020,43.019,47.036,44.031,45.014,46.08,13.037,42.025,30]heptatetraconta-2(3),4,6(47),8(9),10,12,14(15),16,18(46),20(43),21,23(44),25(26),27,29,31(45),32,34,37-(42),38,40-henicosaene (DBTN-2) based on organic boron with a highly twisted fused π-conjugated molecular design. This design concept significantly reduced the relaxation energy between the excited state and the ground state geometries, resulting in an FWHM of only 20 nm.[27] Lee and colleagues improved the rigidity, and resonance strength, suppressed molecular bending and twisting, and destabilized the HOMO energy by intramolecular cyclization in the carbonyl/N resonant core. This resulted in the formation of a deep blue emitter with a peak wavelength of 440 nm and an ultranarrow bandwidth of 16 nm.[28] In addition, Wu *et al.* performed a detailed theoretical analysis of the recombination energy that characterizes the vibrational coupling strength, elucidating the color purity changes of B, O-doped polycyclic aromatic compounds with MR-TADF. The computational results showed that changes in the bond length played a major role in the recombination energy of these highly conjugated aromatic molecules, and the source of the large recombination energy could be explained from the perspective of molecular orbitals;[29] researchers have also made significant efforts to improve the color purity of TADF molecules.[30–35]

However, there is still a lack of theoretical research on the internal physical factors of FWHM, which hinders a true understanding of the internal mechanisms for improving color purity of luminescence molecules. Therefore, we believe that a time-saving and effective strategy is to fundamentally understand the influencing factors of FWHM through theoretical analyses.

Recently, Zheng *et al.* effectively synthesized TADF conjugates of carbazole/carbonyl through the addition and cyclization reaction of cyanide with carbazole. The attachment of auxiliary donors (including carbazole, diphenylamine, and phenolazine) to the carbazole/carbonyl backbone further shifted their emissions from blue to yellow-green. It is worth mentioning that a pure blue OLED with a peripheral carbazole-attached emission layer had a maximum external quantum efficiency (EQE_{max}) of 22.3% and FWHM of 48 nm.[36] Based on this point, detailed theoretical calculations and analyses were performed for these three molecules (shown in Fig. 1), the energy consumption processes of excited states are fully revealed, and the influence of the donor groups on the FWHM of vibrational resolved TADF spectra is illustrated. The results show that molecules with charge transfer (CT) states exhibit larger FWHM, while molecules with hybridized local charge-transfer (HLCT) states have smaller FWHM. Moreover, the relationship between FWHM and reorganization energy is explored, and low reorganization energies contribute to the reduction in FWHM. Additionally, the electron-donating ability of the donor group affects the spectral broadening, with weaker abilities resulting in narrower spectra. Thus, a wise strategy to achieve narrowband thermally activated delayed fluorescence emission by constructing a shallow

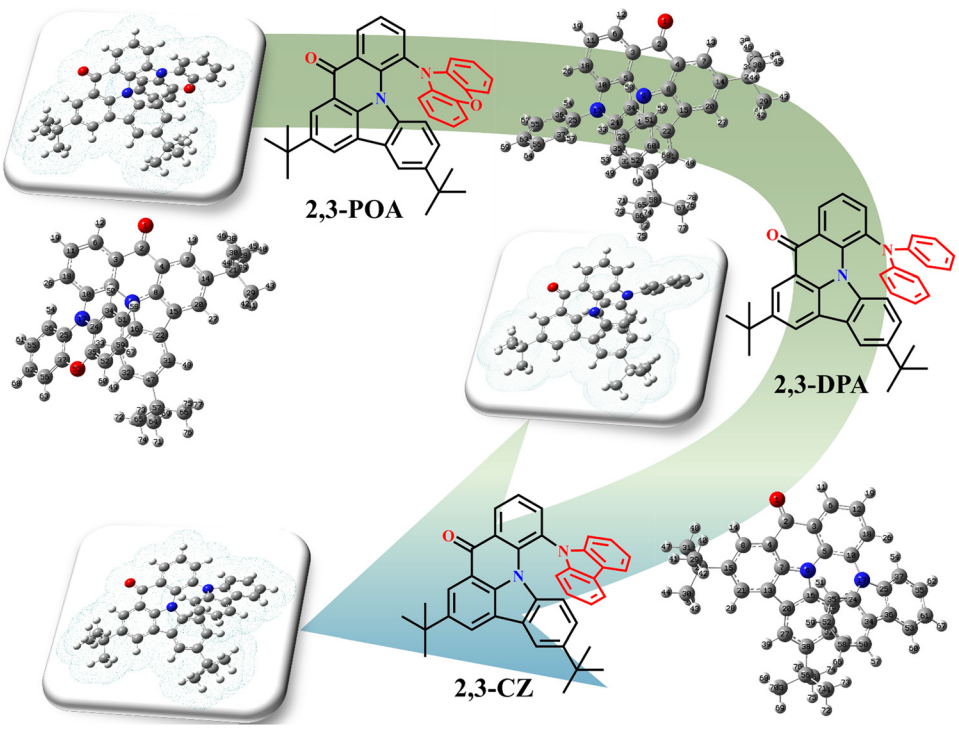

Fig. 1 Molecular structures and PCM models (in toluene) of 2,3-POA, 2,3-DPA, and 2,3-CZ. The atomic numbers are also being displayed in the figure.

potential energy surface for the ground state is theoretically proved and proposed.

2. Theoretical derivations from FWHM to PES for the ground state

Let us start by reviewing the Golden rule expression for the molar absorptivity of the transition from the r state to the p state. Neglecting the coordinate dependence of the optical dipole matrix element, the molar absorbance ε_ν, denoted by $-\log I/I_0 = \varepsilon_\nu ML$, is defined as the ratio of the incident light intensity (I_0) to the transmitted light intensity (I) multiplied by the molar concentration (M) of the solute and the path length (L).

Next, we turn to the quantum expression. In the Golden rule expression for the electron-transfer rate constant and that for absorbance ε_ν/ν or fluorescence f_ν/ν^3 quantum expression when the Condon approximation is introduced:[37,38]

$$\varepsilon_\nu/\nu = (C_a/\delta_\nu)\sum_{n,m}\left|\langle\psi_n^p|\psi_m^r\rangle\right|^2 e^{-E_n^r/k_BT} \quad (1)$$

There into:

$$h\nu \le E_m^p - E_n^r + \Delta E_{rp}^0 \le h(\nu+\delta_\nu) \quad (2)$$

E_m^p and E_n^r represent the mth and nth energy levels of the p and r electronic states, respectively, measured relative to their respective lowest states considering nuclear motion. ψ_n^p and ψ_m^r are the wave functions for the nuclear motion on the p and r surfaces, respectively. ΔE_{rp}^0 represents the adiabatic energy difference between the r-state and p-state. Similarly, for the fluorescence spectrum of the transition from the p-state to the r-state, the probability of emitting photons in the frequency range per unit time (ν, $\nu+\delta_\nu$) is denoted as $f_\nu\delta_\nu$:

$$f_\nu/\nu^3 = (C_f/\delta_\nu)\sum_{n,m}\left|\langle\psi_n^p|\psi_m^r\rangle\right|^2 e^{-E_n^r/k_BT} \quad (3)$$

In (1) C_a is given by:[39]

$$C_a = 8\pi^3 N_A'\left|\mu_{rp}\right|^2/(3hncQ_r\ln 10) \quad (4)$$

where N_A' denote Avogadro's number divided by 10^3, μ_{rp} represent the transition dipole matrix element for the r → p transition. n, c, and Q_r denote the refractive index of the medium, the velocity of light, and the partition function of the system when the solute is in the r electronic state.

Similarly,

$$C_f = 64\pi^4 n|\mu_{rp}|^2/ehc^3Q_p \quad (5)$$

where Q_p denotes the partition function of the entire system with the solute in the p electronic state.

Expanding eqn (1) yields:

$$\varepsilon_\nu/\nu = C_a\sum_{m,n}\left|\langle\varphi_n^r||\varphi_m^p\rangle\right|^2 e^{-G_r^s(x)/k_BT}p_n(T)(dx/d\nu)\Big/\int_{-\infty}^{\infty}e^{-G_r^s(x)/k_BT}dx \quad (6)$$

where $|\langle\varphi_n^r|\varphi_m^p\rangle|^2$ is the Franck–Condon factor for the vibrational mode, and $p_n(T)$ is the equilibrium probability of the solute in the n vibrational level of the electronic state r. $G_r^s(x)$ is the equilibrium solvation free energy for the r-state. In the case of weak electronic coupling between the r-state and p-state:[40]

$$k_{rp}^{ET}\Big/k_{rp}^{ET,max} = e^{-\Delta G_{rp}^*(q^*)/k_BT} \quad (7)$$

$$(\varepsilon_\nu/\nu)/(\varepsilon_\nu/\nu)_{max} = e^{-\Delta G_{rp}^*(q^*)/k_BT} \quad (8)$$

where $\Delta G_{rp}^*(q^*)$ is the reorganization energy on the electronic r-state. Combining eqn (7) and (8) yields:

$$k_{rp}^{ET}\Big/k_{rp}^{ET,max} = (\varepsilon_\nu/\nu)/(\varepsilon_\nu/\nu)_{max} \quad (9)$$

Finally, the expression for the FWHM of the fluorescence spectrum is:

$$W_f \simeq 2[(\lambda_i^r\hbar\omega_r + 2\lambda_0 k_BT + 2\lambda_i k_BTk_r/k_p)(2\ln 2)]^{1/2} \quad (10)$$

where λ_i^r is the "vibrational reorganization parameter". $\hbar\omega_r$ is the spacing of energy levels in the r states. λ_0 is a second solvent contribution. k_r/k_p denotes the ratio of the force constant in the equilibrium solvation-free energy of r and p states. It is evident from the abovementioned equations that nuclear motion wavefunctions can influence the reorganization energy of lower energy states, thereby affecting the FWHM of the emission spectrum. Moreover, considering the TADF process that we are investigating, we believe that the reorganization energy of the S_0 state has a significant impact on the FWHM.

Based on the total spontaneous emission rate:[41,42]

$$K_r = \int\frac{4\omega^3}{3\hbar c^3}\sum_{r,p}P_r\left|\mu_{pr}\right|^2\delta(\omega_{rp}-\omega)d\omega \quad (11)$$

Considering radiation occurring between two electronic states and under the adiabatic approximation with $P_r = P_r(T)$ taken as the Boltzmann distribution, eqn (11) can be written as:

$$K_r(T) = \int\sigma_f(\omega,T)d\omega \quad (12)$$

where:

$$\sigma_f(\omega,T) = \frac{4\omega^3}{3\hbar c^3}\sum_{\nu_r,\nu_p}P_{r\nu_r}(T)\left|\left\langle\psi_{p,\nu_p}\left|\mu_{pr}\right|\psi_{r,\nu_r}\right\rangle\right|^2\delta(\omega_{r\nu_r p\nu_p}-\omega) \quad (13)$$

$\sigma_f(\omega,T)$ represent the differential radiation rate. $|\psi_{r\nu_r}\rangle$ and $|\psi_{p\nu_p}\rangle$ represent the Born–Oppenheimer adiabatic states. From eqn (11)–(13), it is also evident that the nuclear motion wavefunction has an impact on the spontaneous emission rate. It is well known that the nuclear motion wavefunction and the potential energy surface mutually influence each other. The shape and parameters of the potential energy surface affect the form and energy level distribution of the nuclear motion wavefunction, whereas the form and energy level distribution of the nuclear motion wavefunction, in turn, affect the shape of the potential energy surface. This interaction allows the

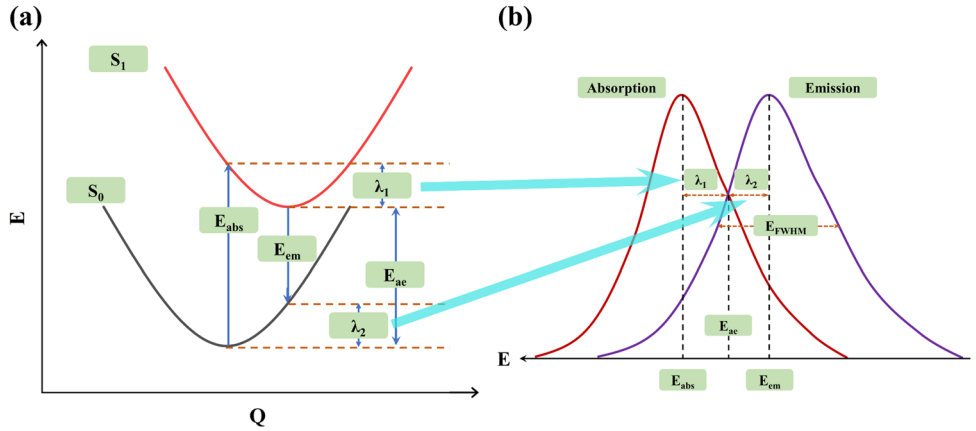

Fig. 2 (a) Potential energy surfaces of the S_0 and S_1 states and (b) schematic representation of the absorption and emission spectra.

potential-energy surface and the nuclear motion wavefunction to jointly describe the molecular structure and dynamics in quantum chemistry. Based on the above, we can come to the following conceptions:

Based on the aforementioned analyses, we now explain this issue using a more easily understandable approach. As is commonly known, the energy value of a system corresponds to the molecular geometric structures, and the energy values at different nuclear coordinates together form the potential energy surface (PES). Therefore, PES serves as a pivotal means for investigating the internal mechanisms of molecules.[43–48] According to Marcus's theory, λ_1 and λ_2 represent the different reorganization energies (shown in Fig. 2(a)). If we express the abscissa of the spectrum as energy E, the absorption and emission spectra of the organic luminescence molecules are illustrated in Fig. 2(b). It is evident that the broadening of the absorption spectrum is primarily associated with λ_1 on the S_1 PES, while the broadening of the emission spectrum is mainly influenced by λ_2 on the S_0 PES. Therefore, the relationships between FWHM and PES for the ground state are established, and our subsequent discussion primarily focuses on the S_0 PES.[48–58]

3. Computational details

To better describe the photophysical properties of TADF molecules in the liquid phase, a PCM computational model was established.[59–62] Additionally, the excited-state properties are highly sensitive to the choice of functional. In addressing this issue, different functionals such as B3LYP, BMK, M062X, PBE0, and WB97XD were employed to calculate the emission wavelengths in the liquid phase, and the results are presented in Table 1. It is observed that the PBE0 functional exhibited excellent agreement with the experimental values for all the studied molecules. Therefore, our subsequent calculations were performed based on the PBE0 functional coupled with the 6-31g(d) basis set. In the calculations, both the ground state and excited state geometric and electronic data were obtained using the density functional theory (DFT) and time-dependent density functional theory (TD-DFT) methods, respectively.

Table 1 Emission wavelengths (nm) of S_1 calculated by different functionals for 2,3-CZ, 2,3-DPA and 2,3-POA in toluene

		B3LYP	BMK	M062X	PBE0	WB97XD	Exp[a]
S_1	2,3-CZ	470.81	395.93	371.66	443.10	359.93	449
	2,3-DPA	524.29	431.87	402.38	492.00	391.78	496
	2,3-POA	649.73	493.58	431.86	598.02	399.75	547

[a] Emission peak at room temperature measured in toluene (5.0×10^{-5} m).

All the above-mentioned calculations were carried out using the Gaussian16 package.[63] In order to investigate the excited state energy consumption processes of these TADF molecules, the radiative decay rate (k_r) was calculated based on Einstein's spontaneous emission equation with the expression of $k_r = -E^2 f/1.499\ s^{-1}$. The non-radiative decay rate (k_{nr}) is determined using the thermal vibration correlation function (TVCF) theory method, obtained through the MOMAP program, with a Lorentzian broadening width of 100 cm^{-1}.[64] Furthermore, the spin–orbit coupling (SOC) constants were calculated using the Dalton 2013 program,[65] based on fully optimized geometric and electronic data. In addition, the normal mode analyses for reorganization energies were performed using the DUSHIN package.[66] The vibrational resolved TADF spectra are simulated using the TVCF spectral theory implemented in the MOMAP program. All these related equations and processes can be found in Peng, Shuai, Cui, Ma, Bai, and our works.[67–70] Besides, the vibration-mode mixing effect can be taken into account as $Q_{ik} = \sum_{l}^{3n-6} S_{kl} Q_{fl} + D_k$. Here, S is the Duschinsky rotation matrix representing the mixing of normal modes in the initial and final states and the vector D_k is the displacement along the normal mode k. All these parameters and reorganization energies can be projected onto the internal coordinates using Reimers' algorithm.[71,72]

4. Results and discussion

4.1. Impact of donor groups on FWHM

Firstly, as depicted in Fig. 3, we calculated the spectral full width at half maximum of the three molecules by setting

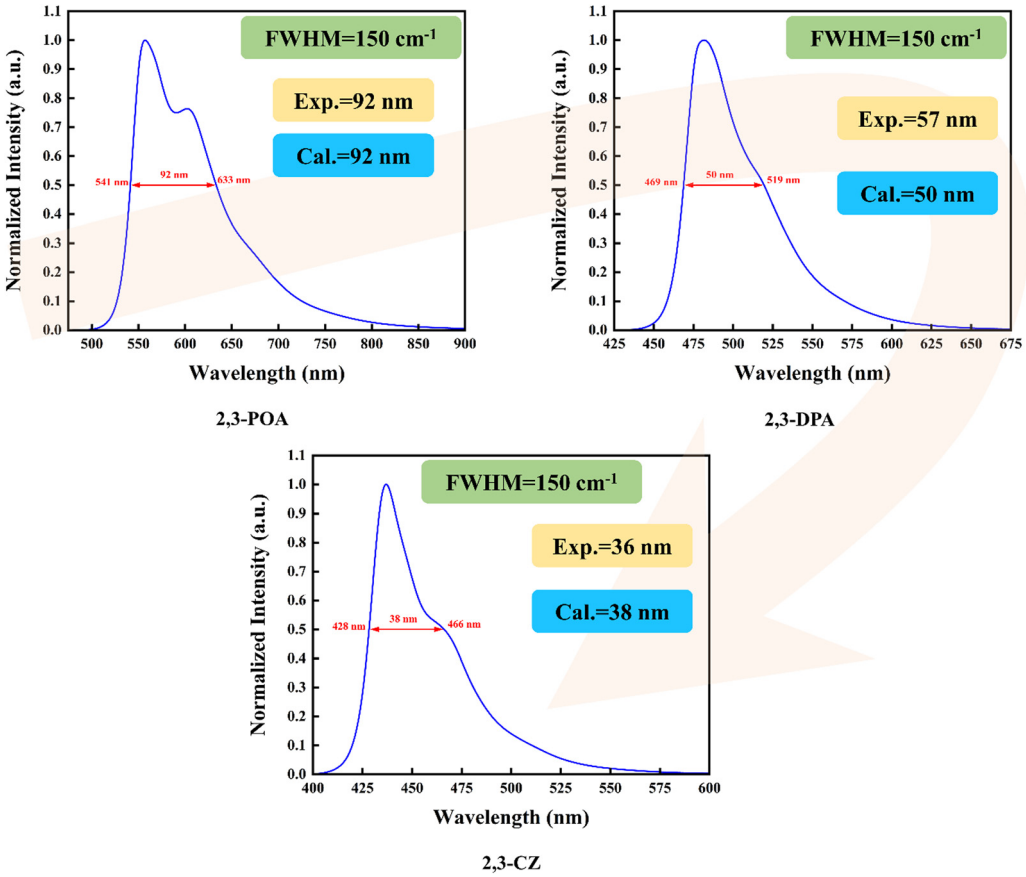

Fig. 3 Calculated phosphorescence spectra in toluene at room temperature.

FWHM = 150 cm^{-1}, resulting in values of 92 nm, 50 nm, and 38 nm. We then compared our calculated values with the corresponding experimental data obtained from ref. 36, which were 92 nm, 57 nm, and 36 nm, respectively. A close correspondence between our calculated and experimental values is evident. By analyzing the data, we observed that the 2,3-POA molecule has the largest FWHM (96 nm), followed by the 2,3-DPA molecule with an FWHM of 52 nm, while the 2,3-CZ molecule exhibited the smallest FWHM, measuring 40 nm. This indicates that the different donor groups could generate significant influence on FWHM. Later, we calculated the absorption spectra of the three molecules in toluene, and the corresponding results are shown in Fig. S1 (ESI†). The results reveal distinct absorption peaks at different wavelengths for each molecule. Specifically, 2,3-POA exhibits an absorption peak at 494 nm, 2,3-DPA at 454 nm, and 2,3-CZ at 418 nm. Moreover, to provide a better understanding of their photophysical properties, we conducted a molecular frontier orbital analysis. The energy and distribution of the orbitals are depicted in Fig. S2–S4 (ESI†). It is evident that the S_0 and S_1 states of the investigated molecule were primarily governed by the transition of the highest occupied molecular orbital (HOMO) to the lowest unoccupied molecular orbital (LUMO). Similarly, the T_1 state of 2,3-POA was also dominated by the HOMO → LUMO transition. The T_2 state of 2,3-DPA is predominantly influenced by the HOMO−1 → LUMO transition (68.9%), in addition to the transitions involving HOMO → LUMO (11.3%) and HOMO−8 → LUMO (4.4%). The T_3 state of 2,3-CZ is mainly influenced by the HOMO−1 → LUMO transition (44.2%), along with the transitions involving HOMO → LUMO (22.8%), HOMO−2 → LUMO (8.5%), and HOMO−7 → LUMO (8.9%).

In order to elucidate the reasons behind these differences, we first analyzed the electronic structures of the three molecules, which revealed the impact of different donor groups on the transition properties. The natural transition orbitals (NTOs) of the S_1 state for the three molecules are illustrated in Fig. 4. Here, we know that the S_1 state of 2,3-POA exhibits a typical CT feature with the LE (local excitation) proportion of 21.31%, which corresponds to a larger FWHM. On the other hand, 2,3-DPA and 2,3-CZ displayed typical HLCT features, with LE proportions of 40.96% and 47.66%, respectively, resulting in smaller FWHM. Based on this, we hypothesize that a large LE proportion in the S_1 state is advantageous in reducing FWHM, 2,3-DPA, and 2,3-CZ with HLCT features favoring to possess small FWHM values (52 nm and 40 nm, respectively) compared with that of 2,3-POA (96 nm). At the same time, we performed analysis of the T-state NTOs, as depicted in Fig. 4. The findings demonstrated that the T_1 state of 2,3-POA corresponded to a CT state, the T_2 state of 2,3-DPA corresponded to an HLCT state,

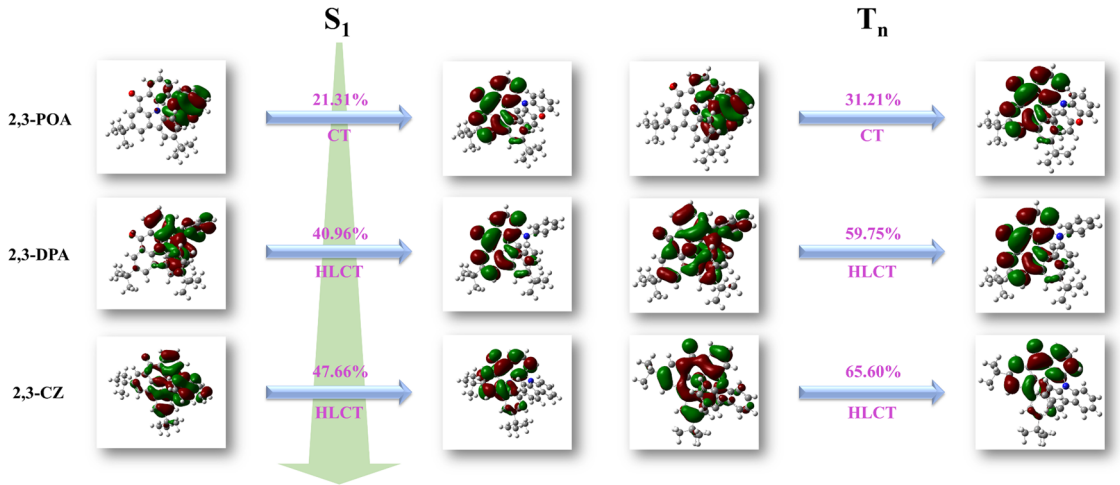

Fig. 4 Natural transition orbitals (NTOs) of the S_1 state for 2,3-POA, 2,3-DPA, and 2,3-CZ, as well as T_1 state for 2,3-POA, T_2 state for 2,3-DPA, and T_3 state for 2,3-CZ in toluene.

and the T_3 state of 2,3-CZ also corresponded to an HLCT state, exhibiting similarities with the transition properties of the S_1 state. Notably, the S_1 state of 2,3-POA exhibited a 21.31% from LE proportion, whereas the T_1 state displayed a 31.21% LE proportion, indicating a difference of 9.90%. Similarly, the S_1 state of 2,3-DPA manifested a 40.96% LE proportion, while the T_2 state exhibited a 59.75% LE proportion, signifying a difference of 18.79%. Likewise, the S_1 state of 2,3-CZ showcased a 47.66% LE proportion, whereas, the T_3 state revealed a 65.60% LE proportion, indicating a difference of 17.94%. Based on these observations, it can be inferred that the S_1 and T_1 states of 2,3-POA exhibited the smallest SOC, whereas the SOC between

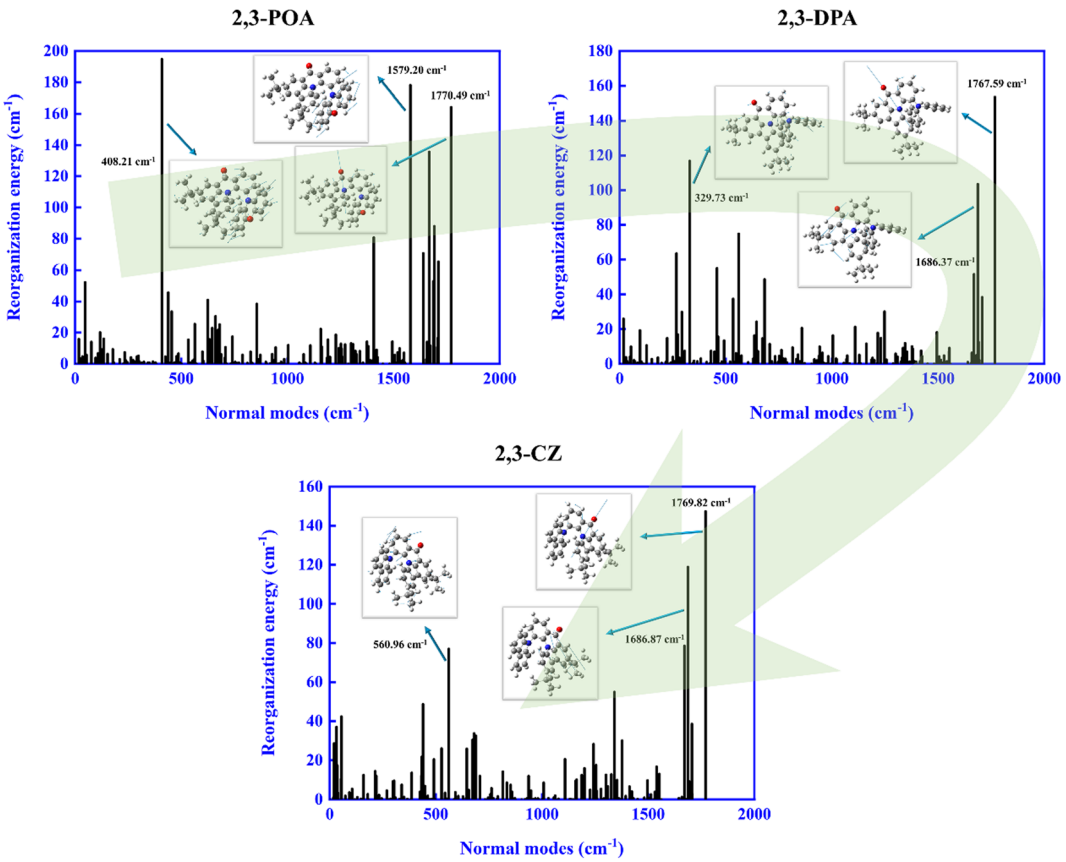

Fig. 5 Calculated reorganization energies *versus* the normal mode frequencies for 2,3-POA, 2,3-DPA, and 2,3-CZ in toluene, respectively. Representative vibration modes are shown as insets.

the S_1 and T_2 states of 2,3-DPA, and between the S_1 and T_3 states of 2,3-CZ, were of similar magnitudes.

Furthermore, as mentioned in Section 2, the FWHM is closely related to the reorganization energy of the ground state. Ideally, eliminating all vibrational transitions except for the main emission peak is desirable; however, due to the redistribution of charges in the S_1 state, it is not possible to completely restrict structural changes. Therefore, the molecular design of narrowband emitting TADF molecules requires smaller reorganization energies. Similarly, we speculate that 2,3-CZ has the smallest reorganization energy. Based on this point, we analyzed the reorganization energies of the three molecules, and the corresponding results are shown in Fig. 5. As we speculated, the reorganization energy of 2,3-POA is the highest with large contributions from high-frequency modes. Therefore, we believe that changes in the bond length significantly contribute to the reorganization energy. Moreover, the reorganization energy of 2,3-DPA is smaller, while the reorganization energy corresponding to the same high-frequency modes remains larger. As for 2,3-CZ, the reorganization energy is the smallest. Hence, we conclude that small reorganization energies are advantageous in reducing FWHM. Subsequently, we analyzed the contributions from bond length, bond angle, and dihedral angle to the reorganization energy, and the corresponding results are shown in Fig. S5 (ESI†) and the calculated data are summarized in Table 2. We find that for all three molecules, bond lengths contribute the most, accounting for 62%, 47%, and 53%, respectively. Furthermore, to reveal the effect of different donor groups on reorganization energies, reorganization energy contributions from the bond length in the donors of 2,3-POA, 2,3-DPA, and 2,3-CZ were analyzed, and the corresponding results are shown in Table S1 (ESI†). We know that the bond lengths between atoms 17 and 24 as well as between atoms 17 and 25, exhibited significant contributions.

Based on this issue, we calculated the potential energy curves for the bond lengths between atoms 17–24 and 17–25 for the three molecules, corresponding results are shown in Fig. 6 and 7, respectively. As mentioned earlier, the FWHM is closely related to the reorganization energy on the S_0 potential energy surface. Therefore, we focus on the S_0 potential energy surface. From Fig. 6, we can see that 2,3-POA has the largest variation in reorganization energies attributed to changes in the bond length (λ_2) value of 0.014 eV, followed by 2,3-DPA with 0.005 eV, and 2,3-CZ has the smallest λ_2 value of 0.003 eV. Similarly, from Fig. 7, a similar pattern is determined with λ_2 values of 0.011 eV, 0.002 eV, and 0.001 eV for 2,3-POA, 2,3-DPA, and 2,3-CZ, respectively. This result perfectly corresponds to the previously mentioned pattern of FWHM. Therefore, we conclude that the emission spectral broadening of these three molecules is primarily related to the variation in the bond lengths of the donor groups. In addition, we conducted simultaneous potential energy surface scans for the bond lengths between the 17th and 24th atoms, as well as between the 17th and 25th atoms, in the S_0, S_1, and T_1 states of the three molecules, and the obtained results are shown in Fig. S6 (ESI†). The findings demonstrate that all three molecules exhibit a single minimum energy configuration across the S_0, S_1, and T_1 states, and no additional structures are discovered.

In addition, if there is little or no nuclear displacement between the ground state and the excited state, indicating the same configurations, the 0–0 transition dominates, as depicted

17-24

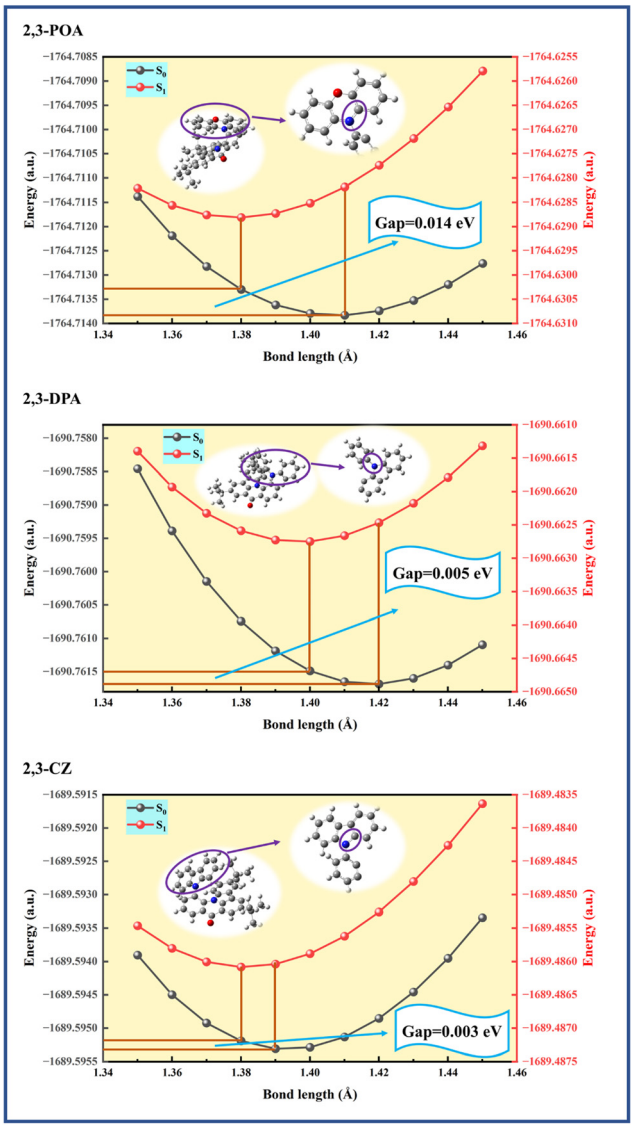

Fig. 6 Potential energy curve of bond length between atom 17 and atom 24 for 2,3-POA, 2,3-DPA, and 2,3-CZ in toluene.

Table 2 Reorganization energies (cm^{-1}) for 2,3-POA, 2,3-DPA and 2,3-CZ from the bond length, bond angle and dihedral angle in toluene, respectively

	Reorganization energy (cm^{-1})			
	Bond length	Bond angle	Dihedral angle	Total
2,3-POA	1216.28	497.85	247.47	1961.60
2,3-DPA	649.32	442.55	293.17	1385.04
2,3-CZ	719.31	316.44	321.68	1357.43

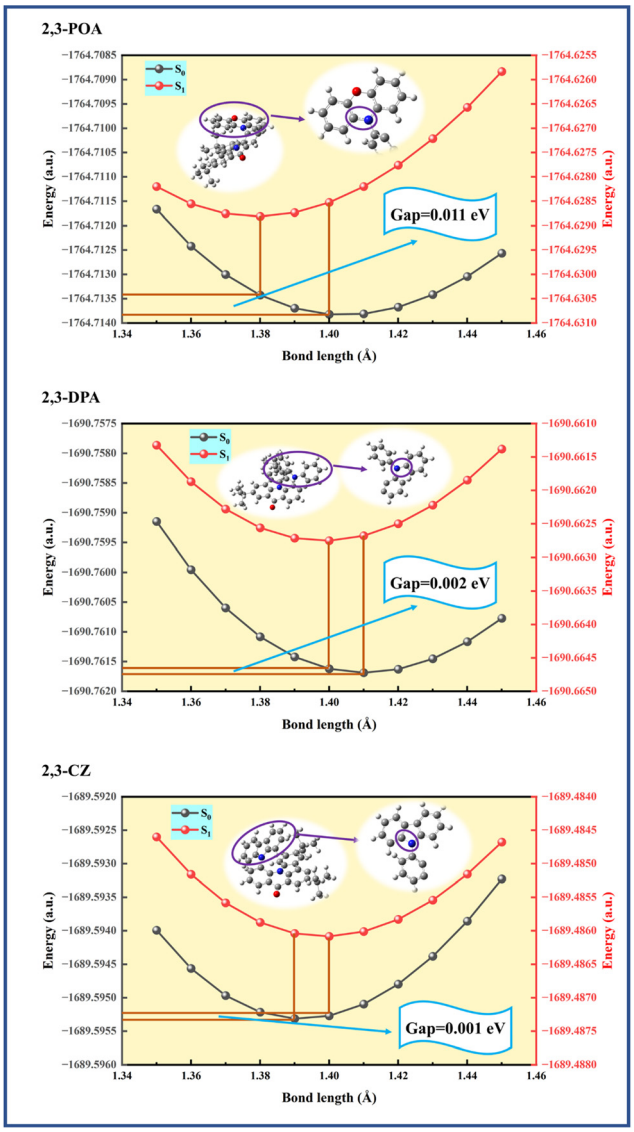

Fig. 7 Potential energy curve of bond length between atom 17 and atom 25 for 2,3-POA, 2,3-DPA, and 2,3-CZ in toluene.

in Fig. S9(b) (ESI†). Conversely, if there is a significant nuclear displacement, signifying a large configuration difference, the scenario illustrated in Fig. S9(a) (ESI†) emerges, where the 0–0 transition deviates from the highest peak. Furthermore, the larger the deviation, the greater the configuration difference between the two states. Based on this, we employ FCclasses3 to calculate the vibrational resolved spectra of the three molecules and annotate the distance between the 0–0 transition and the highest peak, as shown in Fig. 8. The figure reveals that the discrepancy between the 0–0 transition and the highest peak is 9.51 nm for 2,3-POA, 8.6 nm for 2,3-DPA, and 3.96 nm for 2,3-CZ. Consequently, we posit that smaller nuclear displacement corresponds to a smaller FWHM, aligning with the conclusion obtained from Scheme 1.

Subsequently, we focussed on the effect of different donor groups, and the interfragment charge transfer (IFCT) of the electrons between the acceptor and donor was calculated. The obtained data are listed in Table 3. The results showed that 2,3-POA exhibited the strongest electron-donating ability (0.92998), while 2,3-DPA had a weaker electron-donating ability (0.68018), and 2,3-CZ had the weakest electron-donating ability (0.48306).

Thus, based on these analyses, we conclude that a donor group with weaker electron-donating ability is more favorable for achieving a narrower spectral broadening in TADF emission. Moreover, a wise strategy to achieve narrowband emission by constructing a shallow potential energy surface for the ground state is theoretically proved and proposed.

4.2. Excited state dynamics of the TADF molecules

To investigate the TADF properties of these three molecules, the geometric and electronic structures of the ground and excited states were fully optimized, and the corresponding energy landscapes are shown in Fig. S7 (ESI†). Results indicate that 2,3-POA had a small energy difference between its S_1 and T_1 states, measuring 0.06 eV. Similarly, 2,3-DPA has a small energy difference between its S_1 and T_2 states, measuring 0.01 eV, while 2,3-CZ has a small energy difference between its S_1 and T_3 states, measuring 0.03 eV. We then conducted vertical excitation energy calculations for 2,3-CZ, as illustrated in Fig. S8 (ESI†). The S_1 state exhibits a vertical excitation energy of 3.13 eV, whereas the T_1, T_2, T_3, and T_4 states possess energies of 2.68 eV, 2.91 eV, 3.11 eV, and 3.25 eV, respectively. It is evident that the energy of the T_3 state is lower than that of the S_1 state, while the energy of the T_4 state is higher. Therefore, the related SOC constants, intersystem crossing (ISC), and reverse intersystem crossing (RISC) rates were calculated, and the corresponding results are shown in Table 4. The dominant SOC constants of 0.06 cm^{-1}, 0.77 cm^{-1}, and 0.77 cm^{-1} are determined for 2,3-POA, 2,3-DPA, and 2,3-CZ, respectively. Thus, the measured RISC rates are also promising with 2.65×10^5 s^{-1}, 2.94×10^8 s^{-1}, and 5.24×10^6 s^{-1}, respectively. Thus, these findings demonstrate the favorable TADF properties of 2,3-POA, 2,3-DPA, and 2,3-CZ, as evidenced by their small energy differences between the relevant states, significant SOC constants, and efficient RISC rates.

Furthermore, to investigate the energy consumption process, the transition dipole moments, oscillator strengths, and radiative and non-radiative decay rates of the three molecules were theoretically calculated, all these results are listed in Table 5. We know that 2,3-POA exhibits the smallest transition dipole moment of 0.87 Debye, while 2,3-DPA possesses a larger value of 2.22 Debye, and 2,3-CZ has the highest transition dipole moment of 2.69 Debye. The oscillator strengths followed a similar pattern, measuring 0.006, 0.047, and 0.077, respectively. Based on these values, we can anticipate the trends in radiative decay rates, which are also confirmed by the calculations. Specifically, 2,3-POA exhibited the lowest radiative rate of 1.10×10^6 s^{-1} and 2,3-CZ demonstrated the highest rate of 2.62×10^7 s^{-1}. Additionally, 2,3-CZ displayed a relatively lower non-radiative decay rate of 5.72×10^7 s^{-1}. Consequently, we conclude that 2,3-CZ exhibits a higher luminescence efficiency.

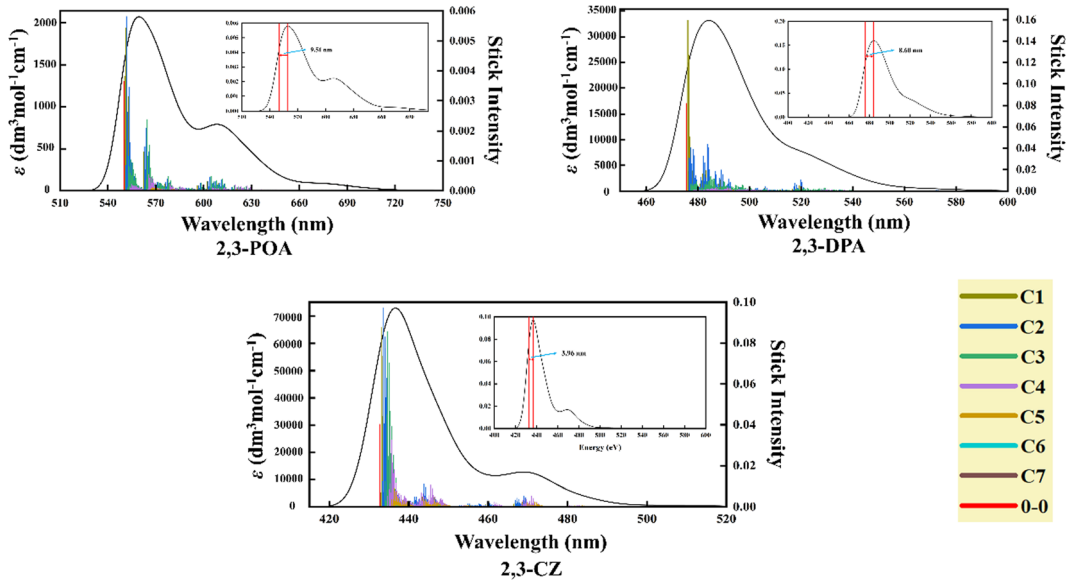

Fig. 8 Emission spectra of the sample are shown, with the vibrational levels represented by C1–C7. The spectra are fitted using a Lorentzian function with a HWHM of 0.036 eV.

Scheme 1 Relationship between the basic physical parameters and FWHM.

Table 3 Interfragment charge transfer (IFCT) of electrons between acceptor (A) and donor (D)

	A → D	D → A	Net D → A
2,3-POA	0.00053	0.93052	0.92998
2,3-DPA	0.00393	0.68411	0.68018
2,3-CZ	0.00409	0.48714	0.48306

Table 4 Calculated ISC and RISC processes and SOC constants (cm^{-1}) among S_1, T_1, T_2 and T_3 for 2,3-POA, 2,3-DPA and 2,3-CZ in toluene

2,3-POA	$\langle S_1\|\hat{H}_{so}\|T_1\rangle$	$k_{ISC(S_1\rightarrow T_1)}$ (s^{-1})	$k_{RISC(T_1\rightarrow S_1)}$ (s^{-1})
	0.06	1.64×10^6	2.65×10^5
2,3-DPA	$\langle S_1\|\hat{H}_{so}\|T_2\rangle$	$k_{ISC(S_1\rightarrow T_2)}$ (s^{-1})	$k_{RISC(T_2\rightarrow S_1)}$ (s^{-1})
	0.77	9.30×10^7	2.94×10^8
2,3-CZ	$\langle S_1\|\hat{H}_{so}\|T_3\rangle$	$k_{ISC(S_1\rightarrow T_3)}$ (s^{-1})	$k_{RISC(T_3\rightarrow S_1)}$ (s^{-1})
	0.77	1.60×10^8	5.24×10^6

As such, the analysis of the transition dipole moments, oscillator strengths, and radiative, and non-radiative decay rates revealed distinct characteristics among the three molecules. Specifically, 2,3-POA demonstrates the smallest transition dipole moment and radiative decay rate, while 2,3-CZ exhibits the largest transition dipole moment and relatively lower non-radiative decay rate, indicating its superior luminescence efficiency.

Table 5 Rate constants of radiative and non-radiative from S_1 to S_0 as well as transition dipole moment (μ) and oscillator strength (*f*) of S_1 for all studied molecules in toluene

	μ (Debye)	*f*	k_r (s^{-1})	k_{nr} (s^{-1})
2,3-POA	0.87	0.006	1.10×10^6	2.58×10^7
2,3-DPA	2.22	0.047	1.30×10^7	5.89×10^7
2,3-CZ	2.69	0.077	2.62×10^7	5.72×10^7

5. Conclusions

In summary, the impact of the donor groups on the FWHM of the vibrational resolved spectra was theoretically studied for the three TADF molecules (2,3-POA, 2,3-DPA, and 2,3-CZ), excited state energy consumption processes were revealed and an efficient strategy to modulate FWHM was proposed. The results showed that 2,3-POA had the largest FWHM of 96 nm, while 2,3-CZ had the smallest FWHM of 40 nm. By analyzing the electronic structures and transition properties, we found that a large LE proportion in the S_1 state is advantageous in reducing the FWHM and that a donor group with weaker electron-donating ability is more favorable for achieving narrowband emission. By analyzing the geometric structures and reorganization energies, we know that small reorganization energies for the S_0 state are beneficial for reducing the FWHM. Moreover, bond lengths (atoms 17–24 and 17–25) in the donor unit exhibited significant contributions to the reorganization energies and generated remarkable influence on the FWHM and TADF properties. In addition, excited state energy consumption processes are revealed by analyzing the radiative and non-radiative as well as ISC and RISC rates, and the superior TADF properties of 2,3-CZ were theoretically verified. Thus, a wise strategy to achieve narrowband TADF emission by constructing

a shallow potential energy surface for the ground state was theoretically proven and proposed. Overall, these findings provide a theoretical perspective to realize mall FWHM and facilitate the development of efficient TADF emitters with high color purity.

Author contributions

Jiaqiang Zhao: writing – original draft; Huanling Liu: data curation; Jianzhong Fan: supervision; Qingfang Mu: writing – review and editing.

Conflicts of interest

There are no conflicts of interest to declare.

Acknowledgements

This work was supported by the National Natural Science Foundation of China (grant no. 62005199, 12204355, and 12274266) and the Natural Science Foundation of Shandong Province (grant no. ZR2020KF017, ZR2021LLZ011, ZR2020 QA072 and ZR2020LLZ001). We thank Professor Yingli Niu for his great help in the usage of MOMAP.

References

1 J. Huo, S. Xiao, Y. Wu, M. Li, H. Tong, H. Shi, D. Ma and B. Z. Tang, Molecular engineering of blue diphenylsulfone-based emitter with aggregation-enhanced emission and thermally activated delayed fluorescence characteristics: impairing intermolecular electron-exchange interactions using steric hindrance, *Chem. Eng. J.*, 2023, **452**, 1385–8947.
2 Y. Shi, H. Ma, Z. Sun, W. Zhao, G. Sun and Q. Peng, Optimal Dihedral Angle in Twisted Donor–Acceptor Organic Emitters for Maximized Thermally Activated Delayed Fluorescence, *Angew. Chem., Int. Ed.*, 2022, **61**, e202213463.
3 X.-K. Chen, D. Kim and J.-L. Brédas, Thermally Activated Delayed Fluorescence (TADF) Path toward Efficient Electroluminescence in Purely Organic Materials: Molecular Level Insight, *Acc. Chem. Res.*, 2018, **51**(9), 2215–2224.
4 Y. Wada, K. Shizu and H. Kaji, Molecular Vibration Accelerates Charge Transfer Emission in a Highly Twisted Blue Thermally Activated Delayed Fluorescence Material, *J. Phys. Chem. A*, 2021, **125**(21), 4534–4539.
5 Y. Im, M. Kim, Y. J. Cho, J.-A. Seo, K. S. Yook and J. Y. Lee, Molecular Design Strategy of Organic Thermally Activated Delayed Fluorescence Emitters, *Chem. Mater.*, 2017, **29**(5), 1946–1963.
6 K. Wang, X.-C. Fan, D.-D. Zhang, Y. Tsuchiya, L. Mei, Y.-Z. Shi, M. Tanaka, Z. Lin, Y.-T. Lee, Y. Xie, Y.-Y. Pan, X. Zhang, W. Liu, G.-L. Dai, J.-X. Chen, B. Wu, J. Zhong, J.-Y. Yuan, C.-J. Zheng, J. Yu, A. K.-Y. Jen, X.-K. Chen, C.-S. Lee, C. Adachi and X.-H. Zhang, Intermolecular pi-pi-packing-induced thermally activated delayed fluorescence: a novel pathway toward luminescence efficiency of nearly 100%, *ChemRxiv*, 2023, preprint, DOI: 10.26434/chemrxiv-2023-wxk36-v2.
7 F.-H. Yu, X.-F. Song, G.-H. Liu, X. Chang, K. Li, Y. Wang, G. Cui and Y. Chen, Highly Efficient Au(I) Alkynyl Emitters: Thermally Activated Delayed Fluorescence and Solution-Processed OLEDs, *Chem. – Eur. J.*, 2022, **28**, e202202439.
8 Y. Xiao, H. Wang, Z. Xie, M. Shen, R. Huang, Y. Miao, G. Liu, T. Yu and W. Huang, NIR TADF emitters and OLEDs: challenges, progress, and perspectives, *Chem. Sci.*, 2022, **13**, 8906–8923.
9 L. Xue, B. Cui, S. Xie and S. Yin, Influence of the Length of the Donor–Acceptor Bridge on Thermally Activated Delayed Fluorescence, *J. Phys. Chem. Lett.*, 2019, **10**(2), 302–308.
10 S. Lin, Q. Ou, Y. Wang, Q. Peng and Z. Shuai, Aggregation-Enhanced Thermally Activated Delayed Fluorescence Efficiency for Two-Coordinate Carbene–Metal–Amide Complexes: A QM/MM Study, *J. Phys. Chem. Lett.*, 2021, **12**(11), 2944–2953.
11 Y.-J. Yu, F.-M. Liu, X.-Y. Meng, L.-Y. Ding, L.-S. Liao and Z.-Q. Jiang, Carbonyl-Containing Thermally Activated Delayed Fluorescence Emitters for Narrow-Band Electroluminescence, *Chem. – Eur. J.*, 2023, **29**, e202202628.
12 J. Liu, Y. Geng, D. Li, H. Yao, Z. Huo, Y. Li, K. Zhang, S. Zhu, H. Wei, W. Xu, J. Jiang and B. Yang, Deep Red Emissive Carbonized Polymer Dots with Unprecedented Narrow Full Width at Half Maximum, *Adv. Mater.*, 2020, **32**, 1906641.
13 C. Lv, X. Wang, Q. Zhang and Y. Zhang, Narrowband emission: organic thermally-activated delayed fluorescence materials and underlying mechanisms, *Mater. Chem. Front.*, 2023, **7**, 2809–2827.
14 J. Chen, X. Xiao, S. Li, Y. Duan, G. Wang, Y. Liao, Q. Peng, H. Fu, H. Geng and Z. Shuai, A Novel Strategy toward Thermally Activated Delayed Fluorescence from a Locally Excited State, *J. Phys. Chem. Lett.*, 2022, **13**(11), 2653–2660.
15 B. C. Garain, S. Das and S. K. Pati, Delineating Conformation Control in the Photophysical Behaviour of a Molecular Donor–Acceptor–Donor Triad, *ChemPhysChem*, 2021, **22**, 2297.
16 Z. Xiong, W. Gong, P. Xu, M. Jiang, X. Cai, Y. Zhu, X. Ping, H. Feng, H. Ma and Z. Qian, Reexamining the heavy-atom-effect: The universal heavy-atom-induced fluorescence enhancement principle for through-space conjugated AIEgens, *Chem. Eng. J.*, 2023, **451**(4), 1385–8947.
17 J. Li, M. Zhang, T. Li, D. Guo, T. Tian and H. Zhang, Realization of switching between TADF and HLCT emissions through modulation of the intramolecular charge transfer character, *J. Mater. Chem. C*, 2022, **10**, 13124–13136.
18 H. Tasaki, S. Shikita, I. S. Park and T. Yasuda, Ester-functionalized thermally activated delayed fluorescence materials, *J. Mater. Chem. C*, 2022, **10**, 4574–4578.
19 H. J. Kim and T. Yasuda, Narrowband Emissive Thermally Activated Delayed Fluorescence Materials, *Adv. Opt. Mater.*, 2022, **10**, 2201714.
20 M. Xie, M. Sun, S. Xue and W. Yang, Recent progress of blue fluorescent organic light-emitting diodes with narrow full width at half maximum, *Dyes Pigm.*, 2023, **208**, 0143–7208.

21 H. Wu, Y.-Z. Shi, K. Wang, J. Yu and X.-H. Zhang, Conformational isomeric thermally activated delayed fluorescence (TADF) emitters: mechanism, applications, and perspectives, *Phys. Chem. Chem. Phys.*, 2023, **25**, 2729–2741.
22 H. Wu, X.-C. Fan, H. Wang, F. Huang, X. Xiong, Y.-Z. Shi, K. Wang, J. Yu and X.-H. Zhang, Conformational isomerization: A novel mechanism to realize the AIE-TADF behaviors, *Aggregate*, 2023, **4**, e243.
23 M. Hasan, A. Shukla, M. Mamada, C. Adachi, S.-C. Lo and E. B. Namdas, Correlating Exciton Dynamics of Thermally Activated Delayed-Fluorescence Emitters to Efficiency Roll-Off in OLEDs, *Phys. Rev. Appl.*, 2022, **18**, 054082.
24 C. Zhao, F. Zhao, K. Wang, H. Yu, T. Huang, R. Wang, C. Zhang, B. Hu and L. Duan, Stabilization of Blue Emitters with Thermally Activated Delayed Fluorescence by the Steric Effect: A Case Study by means of Magnetic Field Effects, *Phys. Rev. Appl.*, 2020, **14**, 034059.
25 Y. Zhang, D. Zhang, J. Wei, Z. Liu, Y. Lu and L. Duan, Multi-Resonance Induced Thermally Activated Delayed Fluorophores for Narrowband Green OLEDs, *Angew. Chem., Int. Ed.*, 2019, **58**, 16912.
26 J. M. Ha, H. B. Shin, J. F. Joung, W. J. Chung, J.-E. Jeong, S. Kim, S. H. Hur, S.-Y. Bae, J.-Y. Kim, J. Y. Lee, S. Park and H. Y. Woo, Rational Molecular Design of Azaacene-Based Narrowband Green-Emitting Fluorophores: Modulation of Spectral Bandwidth and Vibronic Transitions, *ACS Appl. Mater. Interfaces*, 2021, **13**(22), 26227–26236.
27 X.-C. Fan, K. Wang, Y.-Z. Shi, Y.-C. Cheng, Y.-T. Lee, J. Yu, X.-K. Chen, C. Adachi and X.-H. Zhang, Ultrapure green organic light-emitting diodes based on highly distorted fused π-conjugated molecular design, *Nat. Photonics*, 2023, **17**, 280–285.
28 C. Cao, J.-H. Tan, Z.-L. Zhu, J.-D. Lin, H.-J. Tan, H. Chen, Y. Yuan, M.-K. Tse, W.-C. Chen and C.-S. Lee, Intramolecular Cyclization: A Convenient Strategy to Realize Efficient BT.2020 Blue Multi-Resonance Emitter for Organic Light-Emitting Diodes, *Angew. Chem., Int. Ed.*, 2023, **135**, e202215226.
29 W. Cai, C. Zhong and D.-Y. Wu, Achieving high color purity in multi-resonance thermally activated delayed fluorescence emitters through a substitution-driven design strategy, *Mater. Chem. Front.*, 2023, **7**, 3762–3773.
30 Z. Huang, H. Xie, J. Miao, Y. Wei, Y. Zou, T. Hua, X. Cao and C. Yang, Charge Transfer Excited State Promoted Multiple Resonance Delayed Fluorescence Emitter for High-Performance Narrowband Electroluminescence, *J. Am. Chem. Soc.*, 2023, **145**(23), 12550–12560.
31 Y. Gu, X. Sun, M. Wu and K. Wang, Pressure-shortened delayed fluorescence lifetime of solid-state thermally activated delayed fluorescent 4CzIPN: the structure evolution, *Phys. Chem. Chem. Phys.*, 2023, **25**, 17264–17268.
32 J. Liu, Y. Zhu, T. Tsuboi, C. Deng, W. Lou, D. Wang, T. Liu and Q. Zhang, Toward a BT.2020 green emitter through a combined multiple resonance effect and multi-lock strategy, *Nat. Commun.*, 2022, **13**, 4876.
33 X. Cai, J. Xue, C. Li, B. Liang, A. Ying, Y. Tan, S. Gong and Y. Wang, Achieving 37.1% Green Electroluminescent Efficiency and 0.09 eV Full Width at Half Maximum Based on a Ternary Boron–Oxygen–Nitrogen Embedded Polycyclic Aromatic System, *Angew. Chem., Int. Ed.*, 2022, **61**, e202200337.
34 C.-Y. Chan, Y.-T. Lee, M. Mamada, K. Goushi, Y. Tsuchiya, H. Nakanotani and C. Adachi, Carbazole-2-carbonitrile as an acceptor in deep-blue thermally activated delayed fluorescence emitters for narrowing charge-transfer emissions, *Chem. Sci.*, 2022, **13**, 7821–7828.
35 I. S. Park, K. Matsuo, N. Aizawa and T. Yasuda, High-Performance Dibenzoheteraborin-Based Thermally Activated Delayed Fluorescence Emitters: Molecular Architectonics for Concurrently Achieving Narrowband Emission and Efficient Triplet–Singlet Spin Conversion, *Adv. Funct. Mater.*, 2018, **28**, 1802031.
36 X.-F. Luo, F.-L. Li, J.-W. Zou, Q. Zou, J. Su, M.-X. Mao and Y.-X. Zheng, A Series of Fused Carbazole/Carbonyl Based Blue to Yellow-Green Thermally Activated Delayed Fluorescence Materials for Efficient Organic Light-Emitting Diodes, *Adv. Opt. Mater.*, 2021, **9**, 2100784.
37 T. Förster, *Fluoreszenz Organischer Verbindungen*, Vandenhoeck & Ruprecht, Göttingen, 1951.
38 N. Mataga and T. Kubata, *Molecular Interactions and Electronic Spectra*, M. Dekker, New York, 1970.
39 R. A. Marcus, Relation between charge transfer absorption and fluorescence spectra and the inverted region, *J. Phys. Chem.*, 1989, **93**(8), 3078–3086.
40 R. A. Marcus, Nonadiabatic processes involving quantum-like and classical-like coordinates with applications to nonadiabatic electron transfers, *J. Phys. Chem.*, 1984, **81**(10), 4494–4500.
41 Y. Niu, Q. Peng, C. Deng, X. Gao and Z. Shuai, Theory of Excited State Decays and Optical Spectra: Application to Polyatomic Molecules, *J. Phys. Chem. A*, 2010, **114**(30), 7817–7831.
42 Y. Niu, Q. Peng and Z. Shuai, Promoting-mode free formalism for excited state radiationless decay process with Duschinsky rotation effect, *Sci. China, Ser. B: Chem.*, 2008, **51**(12), 1153–1158.
43 B. Zee, Y. Li, G.-J. A. H. Wetzelaer and P. W. M. Blom, Triplet-Polaron-Annihilation-Induced Degradation of Organic Light-Emitting Diodes Based on Thermally Activated Delayed Fluorescence, *Phys. Rev. Appl.*, 2022, **18**(6), 064002.
44 Y. Ning, X. Zhao, F. Wu, Y. Wu, J. Chen, F. Wei, H. Wang, X. Chen and Z. Xiong, Charge-Transfer Dynamics in OLEDs with Coexisting Electroplex and Exciton States, *Phys. Rev. Appl.*, 2023, **19**(6), 064055.
45 K. Vandewal, K. Tvingstedt, A. Gadisa, O. Inganäs and J. V. Manca, Relating the open-circuit voltage to interface molecular properties of donor:acceptor bulk heterojunction solar cells, *Phys. Rev. B: Condens. Matter Mater. Phys.*, 2010, **81**(12), 125204.
46 K. Bergmann, R. Hojo and Z. M. Hudson, Uncovering the Mechanism of Thermally Activated Delayed Fluorescence in Coplanar Emitters Using Potential Energy Surface Analysis, *J. Phys. Chem. Lett.*, 2023, **14**(2), 310–317.

47 M. Kurt, H. Yurtseven, A. Kurt and S. Aksoy, Calculation of the infrared frequency and the damping constant (full width at half maximum) for metal organic frameworks, *Chin. Phys. B*, 2019, **28**(6), 066401.
48 Y. Zhang, D. Zhang, T. Huang, A. J. Gillett, Y. Liu, D. Hu, L. Cui, Z. Bin, G. Li, J. Wei and L. Duan, Multi-Resonance Deep-Red Emitters with Shallow Potential-Energy Surfaces to Surpass Energy-Gap Law, *Angew. Chem., Int. Ed.*, 2021, **60**(37), 20498–20503.
49 K. Zhang, F. Yang, Y. Zhang, Y. Ma, J. Fan, J. Fan, C.-K. Wang and L. Lin, Highly Efficient Near-Infrared Thermally Activated Delayed Fluorescence Molecules via Acceptor Tuning: Theoretical Molecular Design and Experimental Verification, *J. Phys. Chem. Lett.*, 2021, **12**(7), 1893–1903.
50 S. Kundu, P. P. Roy, G. R. Fleming and N. Makri, Franck–Condon and Herzberg–Teller Signatures in Molecular Absorption and Emission Spectra, *J. Phys. Chem. B*, 2022, **126**(15), 2899–2911.
51 F. F. Kong, X. J. Tian, Y. Zhang, Y. J. Yu, S. H. Jing, Y. Zhang, G. J. Tian, Y. Luo, J. L. Yang, Z. C. Dong and J. G. Hou, Probing intramolecular vibronic coupling through vibronic-state imaging, *Nat. Commun.*, 2021, **12**(1), 1280.
52 F. Santoro, A. Lami, R. Improta, J. Bloino and V. Barone, Effective method for the computation of optical spectra of large molecules at finite temperature including the Duschinsky and Herzberg-Teller effect: The Qx band of porphyrin as a case study, *J. Chem. Phys.*, 2008, **128**(22), 24311.
53 W. Cai, H. Zhang, X. Yan, A. Zhao, R. He, M. Li, Q. Meng and W. Shen, What accounts for the color purity of tetradentate Pt complexes? A computational analysis, *Phys. Chem. Chem. Phys.*, 2019, **21**(15), 8073–8080.
54 X. K. Chen, V. Coropceanu and J. L. Brédas, Assessing the nature of the charge-transfer electronic states in organic solar cells, *Nat. Commun.*, 2018, **9**(1), 5295.
55 J. P. Menzel, H. J. de Groot and F. Buda, Photoinduced electron transfer in donor-acceptor complexes: Isotope effect and dynamic symmetry breaking, *J. Phys. Chem. Lett.*, 2019, **10**(21), 6504–6511.
56 Z. R. Grabowski, K. Rotkiewicz and W. Rettig, Structural changes accompanying intramolecular electron transfer: focus on twisted intramolecular charge-transfer states and structures, *Chem. Rev.*, 2003, **103**, 3899–4032.
57 K. Zhang, X. Zhang, J. Fan, Y. Song, J. Fan, C.-K. Wang and L. Lin, Novel Deep Red Thermally Activated Delayed Fluorescence Molecule with Aggregation-Induced Emission Enhancement: Theoretical Design and Experimental Validation, *J. Phys. Chem. Lett.*, 2022, **13**, 4711–4720.
58 S. A. Ahmad, J. Eng and T. J. Penfold, Rapid predictions of the colour purity of luminescent organic molecules, *J. Mater. Chem. C*, 2022, **10**(12), 4785–4794.
59 Y. Song, B. Li, S. Liu, M. Qin, Y. Gao, K. Zhang, L. Lin, C.-K. Wang and J. Fan, Structure–property relationship study of blue thermally activated delayed fluorescence molecules with different donor and position substitutions: theoretical perspective and molecular design, *J. Mater. Chem. C*, 2022, **10**(12), 4723–4736.
60 H. Zou, Y. Ma, H. Liu, Q. Mu, K. Zhang, Y. Song, L. Lin, C.-K. Wang and J. Fan, A QM/MM study on through space charge transfer-based thermally activated delayed fluorescence molecules in the solid state, *J. Mater. Chem. C*, 2022, **10**(2), 517–531.
61 H. Liu, K. Zhang, H. Zou, Q. Mu, X. Wang, Y. Song, L. Lin, C.-K. Wang and J. Fan, A theoretical perspective of the relationship between the structures and luminescence properties of red thermally activated delayed fluorescence molecules, *Phys. Chem. Chem. Phys.*, 2022, **24**(8), 17140–17154.
62 H. Zou, H. Liu, Q. Mu, K. Zhang, Y. Song, L. Lin, Y. Xu, C.-K. Wang and J. Fan, Theoretical perspective for substitution effect on luminescent properties of through space charge transfer-based thermally activated delayed fluorescence molecules, *Spectrochim. Acta, Part A*, 2023, **285**, 121899.
63 M. J. Frisch, G. W. Trucks, H. B. Schlegel, G. E. Scuseria, M. A. Robb, J. R. Cheeseman, G. Scalmani, V. Barone, G. A. Petersson, H. Nakatsuji, X. Li, M. Caricato, A. V. Marenich, J. Bloino, B. G. Janesko, R. Gomperts, B. Mennucci, H. P. Hratchian, J. V. Ortiz, A. F. Izmaylov, J. L. Sonnenberg, D. WilliamsYoung, F. Ding, F. Lipparini, F. Egidi, J. Goings, B. Peng, A. Petrone, T. Henderson, D. Ranasinghe, V. G. Zakrzewski, J. Gao, N. Rega, G. Zheng, W. Liang, M. Hada, M. Ehara, K. Toyota, R. Fukuda, J. Hasegawa, M. Ishida, T. Nakajima, Y. Honda, O. Kitao, H. Nakai, T. Vreven, K. Throssell, J. A. Montgomery Jr., J. E. Peralta, F. Ogliaro, M. J. Bearpark, J. J. Heyd, E. N. Brothers, K. N. Kudin, V. N. Staroverov, T. A. Keith, R. Kobayashi, J. Normand, K. Raghavachari, A. P. Rendell, J. C. Burant, S. S. Iyengar, J. Tomasi, M. Cossi, J. M. Millam, M. Klene, C. Adamo, R. Cammi, J. W. Ochterski, R. L. Martin, K. Morokuma, O. Farkas, J. B. Foresman and D. J. Fox, *Gaussian 16 Rev. A.03*, 2016.
64 Y. Niu, W. Li, Q. Peng, H. Geng, Y. Yi, L. Wang, G. Nan, D. Wang and Z. Shuai, MOlecular MAterials Property Prediction Package (MOMAP) 1.0: a software package for predicting the luminescent properties and mobility of organic functional materials, *Mol. Phys.*, 2018, **116**, 1078–1090.
65 A. Dalton, *Molecular electronic structure program*, **https://daltonprogram.org**.
66 J. R. Reimers, A Practical Method for the use of Curvilinear Coordinates in Calculations of Normal-Mode-Projected Displacements and Duschinsky Rotation Matrices for Large Molecules, *J. Chem. Phys.*, 2001, **115**(20), 9103–9109.
67 Q. Peng, H. Ma and Z. Shuai, Theory of Long-Lived Room-Temperature Phosphorescence in Organic Aggregates, *Acc. Chem. Res.*, 2021, **54**(4), 940–949.
68 H. Ma, Q. Peng, Z. An, W. Huang and Z. Shuai, Efficient and Long-Lived Room-Temperature Organic Phosphorescence: Theoretical Descriptors for Molecular Designs, *J. Am. Chem. Soc.*, 2019, **141**(2), 1010–1015.
69 Z. W. Li, L. Y. Peng, X. F. Song, W. K. Chen, Y. J. Gao, W. H. Fang and G. Cui, Room-Temperature Phosphorescence and Thermally Activated Delayed Fluorescence in the Pd Complex: Mechanism and Dual Upconversion Channels, *J. Phys. Chem. Lett.*, 2021, **12**(25), 5944–5950.

70 Q. Mu, K. Zhang, H. Zou, H. Liu, Y. Song, C.-K. Wang, L. Lin and J. Fan, Theoretical insights into room temperature phosphorescence emission with anti-Kasha behavior in aggregate, *Dyes Pigm.*, 2022, **205**, 110560.
71 J. R. Reimers, A Practical Method for the Use of Curvilinear Coordinates in Calculations of Normal-Mode-Projected Displacements and Duschinsky Rotation Matrices for Large Molecules, *J. Chem. Phys.*, 2001, **115**, 9103–9109.
72 Y. Niu, Q. Peng, C. Deng, X. Gao and Z. Shuai, Theory of Excited State Decays and Optical Spectra: Application to Polyatomic Molecules, *J. Phys. Chem. A*, 2010, **114**, 7817–7831.